Vortex Airy beams directly generated via liquid crystal q-Airy-plates

Bing-Yan Wei, Sheng Liu, Peng Chen, Shu-Xia Qi, Yi Zhang, Wei Hu, Yan-Qing Lu, and Jian-Lin Zhao

Citation: Appl. Phys. Lett. **112**, 121101 (2018); doi: 10.1063/1.5019813
View online: https://doi.org/10.1063/1.5019813
View Table of Contents: http://aip.scitation.org/toc/apl/112/12
Published by the American Institute of Physics

Vortex Airy beams directly generated via liquid crystal q-Airy-plates

Bing-Yan Wei,[1,a)] Sheng Liu,[1] Peng Chen,[2] Shu-Xia Qi,[1] Yi Zhang,[1] Wei Hu,[2] Yan-Qing Lu,[2] and Jian-Lin Zhao[1,b)]
[1]*MOE Key Laboratory of Material Physics and Chemistry under Extraordinary Conditions, and Shaanxi Key Laboratory of Optical Information Technology, School of Science, Northwestern Polytechnical University, Xi'an 710072, China*
[2]*National Laboratory of Solid State Microstructures, College of Engineering and Applied Sciences, and Collaborative Innovation Center of Advanced Microstructures, Nanjing University, Nanjing 210093, China*

(Received 17 December 2017; accepted 8 March 2018; published online 19 March 2018)

Liquid crystal q-Airy-plates with director distributions integrated by q-plates and polarization Airy masks are proposed and demonstrated via the photoalignment technique. Single/dual vortex Airy beams of opposite topological charges and orthogonal circular polarizations are directly generated with polarization-controllable characteristic. The singular phase of the vortex part is verified by both astigmatic transformation and digital holography. The trajectory of vortex Airy beams is investigated, manifesting separate propagation dynamics of optical vortices and Airy beams. Meanwhile, Airy beams still keep their intrinsic transverse acceleration, self-healing, and nondiffraction features. This work provides a versatile candidate for generating high-quality vortex Airy beams. *Published by AIP Publishing*. https://doi.org/10.1063/1.5019813

Optical vortices have drawn extensive attention during the past few decades. Optical vortices are characterized by a helical phase structure, a donut-like intensity distribution, and carry orbital angular momentum (OAM) of $m\hbar$, where m is the topological charge.[1] These features facilitate the usages in optical tweezers,[2] quantum informatics,[3] super-resolution imaging,[4] stimulated-emission-depletion (STED)-inspired laser-lithography,[5] vortex coronagraphs,[6] etc. Airy beams have also been a hot topic especially since their first demonstration in 2007.[7] The properties of nondiffraction, transverse acceleration, and self-healing endow Airy beams with a wide range of applications in particle manipulation,[8] light propagation in atmospheric turbulence,[9] light-sheet microscopy,[10] generation of spatiotemporal light bullets[11] and curved plasma channel,[12] and so on. The combination of these two structured beams, namely, vortex Airy beams (VABs), may play special roles in multi-dimensional optical manipulation, lossless quantum communication, STED-microscopy,[13] and even in some uncharted territories.

Several techniques have been exploited to realize the generation of VABs, which can be mainly divided into two groups. The straightforward way is to illuminate the vortex beam generator with an Airy beam,[14] and vice versa.[15] Another way for directly modulating Gaussian beams is to create composite phase patterns consisting of a singular phase and a cubic[15,16] or 3/2 phase.[17] In these works, either a dielectric metasurface or a spatial light modulator (SLM) is needed. Nevertheless, a time-consuming femtosecond laser writing process is required for the fabrication of metasurfaces. Meanwhile, the element mainly efficiently works for a fixed wavelength, lacking the degree of tunability. The SLM can be flexibly adjusted. However, the beam expansion setup is inevitable for a laser beam to match the size of the SLM chip. Additionally, the SLM is composed of discrete pixels that are driven separately by a complex electrode matrix, decreasing the efficiency (less than 40%)[18] and quality of the output VABs. Therefore, exploiting a versatile approach for VABs' generation is still in high demand.

In this paper, by means of a sulphonic azo-dye SD1 based photoalignment technology and a digital micro-mirror device (DMD) based dynamic exposure process, innovative liquid crystal (LC) q-Airy-plates are demonstrated for generating VABs with high quality and efficiency. Different from our previous work in which the combination of a separate LC q-plate and polarization Airy mask (PAM) method was adopted,[19] to make the optical configuration more compact, we directly integrate the LC director distributions of these two kinds of elements, achieving the q-Airy-plate design. Moreover, polarization-controllable VABs of opposite topological charges and orthogonal circular polarizations are obtained simultaneously with a higher efficiency over 90%. In addition, distinct propagation dynamics reveal separate trajectories of the vortex part and Airy beam. The overall research provides a reference for the fundamental study of VABs and may promote VABs' potential applications mentioned above.

Figure 1 depicts the principle of the q-Airy-plate design. Herein, we take q(0.5)-Airy-plate and q(1)-Airy-plate as examples for better description. Figure 1(a) is the cubic phase pattern (black to white indicates 0 to 2π) with a modulation range of -15π to 15π to generate a 2D Airy beam. On the other hand, when introduced by the geometric phase, it can also be regarded as the optical axis distribution of the PAM,[20] in which black to white indicates the optical axis varying from 0 to π. Figures 1(b) and 1(d) are the optical axis distributions of the q(0.5)-plate and q(1)-plate used to generate $m = 1$ and $m = 2$ optical vortices, respectively.[21] By directly superposing these two types of distributions, we can get the designed optical axis orientation which meets the following equation:

$$\alpha = \frac{\varphi_{CP}}{2} + q\varphi, \tag{1}$$

[a)]Electronic mail: wbyxz@nwpu.edu.cn.
[b)]Electronic mail: jlzhao@nwpu.edu.cn.

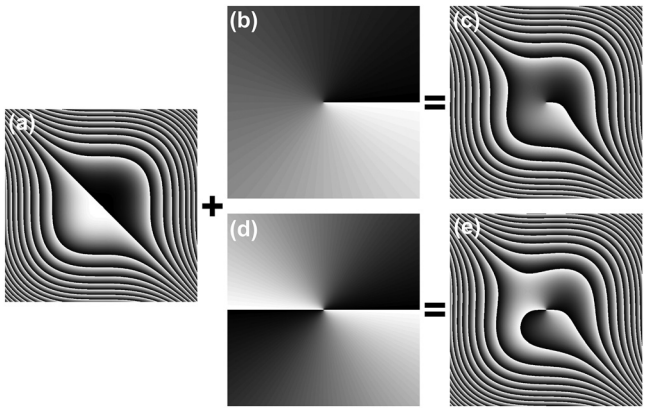

FIG. 1. Principle of the q-Airy-plate design. The optical axis distributions of (a) PAM and (b) q(0.5)-plate/(d) q(1)-plate compose (c) q(0.5)-Airy-plate/(e) q(1)-Airy-plate, respectively. Black to white in all the optical axis distribution patterns indicates the optical axis varying from 0 to π.

where $\varphi_{CP}(x, y) = x^3 + y^3$ is the cubic phase distribution, $q = m/2$ is the half of the topological charge, and $\varphi(x, y) = \arctan(y/x)$ stands for the azimuthal angle. As the first term represents the Airy factor and the second term describes the q-plate, we name the created element q-Airy-plate. The integrated optical axis distributions of the q(0.5)-Airy-plate and q(1)-Airy-plate are shown in Figs. 1(c) and 1(e), respectively. From the patterns, we can see that the spiral structures are obviously introduced, distorting the central orientation of the cubic mask.

The diffraction property of the q-Airy-plate can be analyzed through the Jones calculus. The Jones matrix for this optical element can be expressed by[22]

$$\mathbf{M} = \cos\frac{\Gamma}{2}\begin{bmatrix}1 & 0\\ 0 & 1\end{bmatrix} - i\sin\frac{\Gamma}{2}\begin{bmatrix}\cos 2\alpha & \sin 2\alpha\\ \sin 2\alpha & -\cos 2\alpha\end{bmatrix}, \quad (2)$$

where $\Gamma = 2\pi\Delta nd/\lambda$ is the phase retardation, Δn is the birefringence of the optical material comprising the q-Airy-plate, d is the thickness, and λ is the incident wavelength. When the sample is illuminated by a left/right circularly polarized Gaussian beam, the output light is changed to be

$$\mathbf{E}_{out} = \mathbf{M}\cdot\mathbf{E}_{in} = \mathbf{M}\cdot \mathrm{E}_0\begin{bmatrix}1\\ \pm i\end{bmatrix} = \mathrm{E}_0\cos\frac{\Gamma}{2}\begin{bmatrix}1\\ \pm i\end{bmatrix} - \mathrm{E}_0 i\sin\frac{\Gamma}{2}\exp(\pm i2q\varphi)\exp\left[\pm i(x^3+y^3)\right]\begin{bmatrix}1\\ \mp i\end{bmatrix}, \quad (3)$$

where $\mathbf{E}_{in} = \mathrm{E}_0 \times [1, \pm i]^{\mathrm{T}}$ is the Jones vector of the incident electric field and (+)/(−) corresponds to left/right circular polarization, respectively. Despite the first term, which is the residual component of the incident light and can be eliminated under the half-wave condition, the second term shows that the output field carries the OAM given by $2q\hbar$, reveals the feature of the cubic phase modulation, while exhibits the opposite handedness to the incident polarization. Thus, a VAB with a circular polarization state orthogonal to the incident light will be formed.

Herein, nematic LC E7 is utilized to implement the q-Airy-plate. The photoalignment material, sulphonic azo-dye SD1, is adopted as the alignment agent. Under linearly polarized UV irradiation, the SD1 molecules will orientate perpendicularly to the incident polarization direction.[23,24] This orientation will further spread to adjacent LCs by intermolecular interactions. A DMD based microlithography system[25] is employed to realize the precise duplication of q-Airy-plate patterns to LC cells, which are composed of SD1-spin-coated indium-tin-oxide glass substrates separated by 5 μm spacers. After an eighteen-step five-time-partly overlapping dynamic exposure process[26] taking only 5 min and the capillary filling of E7 to the cells, the fabrication of a director variant LC q-Airy-plate is accomplished. In addition to the inexpensive materials utilized here, less consumption of them is needed as the q-Airy-plate is an integrated configuration, which greatly reduces the fabrication cost.

Figures 2(b) and 2(e) are detected azimuthal director distributions of the LC q(0.5)-Airy-plate and q(1)-Airy-plate, respectively, and they are carried out by a 2D Stokes parameters measurement, which in sequence consists of a polarizer, a $\lambda/4$ plate, a holder for samples, another $\lambda/4$ plate and polarizer, and a CCD to capture optical images for a LabVIEW program executing data calculation.[24,27] Compared to the colored simulations, they match well with Figs. 2(a) and 2(d) accordingly, except for a 90° shift, which is attributed to SD1's perpendicular orientation mentioned above. Due to the limited resolution of the 2D Stokes setup (~10 μm),[27] detailed azimuthal distribution cannot be accurately reflected. In fact, LC directors vary periodically and continuously, which can be proved by the micrographs in the third column of Fig. 2. As the samples are observed under a polarized optical microscope, the bright areas of the micrographs reveal that the angle between the LC directors and the polarizer is ~45° or 135°, while that of the dark areas is ~0° or 90°.[28] The reddish color results from the corresponding wavelength that satisfies the half-wave condition.[29] Thus, during the directors changing from 0° to 180°, the bright-to-dark alternates twice, leading to microscopic images with denser fringes. However, the consecutive variation of the brightness confirms the continuous orientation of LC molecules as designed.

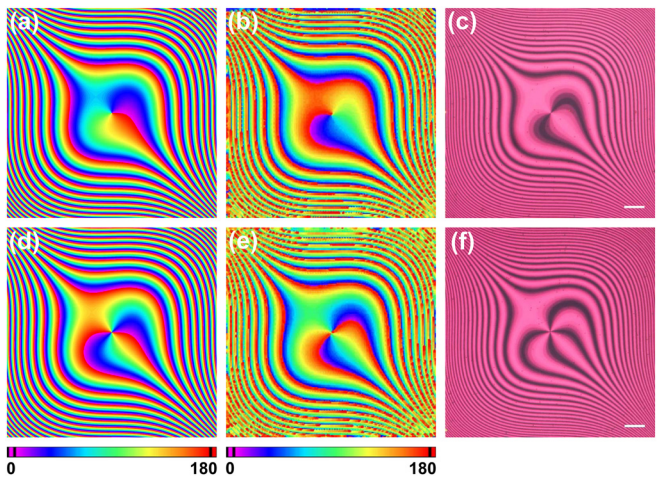

FIG. 2. (a) and (d) Simulated and (b) and (e) measured LC azimuthal director distributions and (c) and (f) micrographs of the q(0.5)-Airy-plate and q(1)-Airy-plate, respectively. The color bars indicate the corresponding LC director varying from 0° to 180°. The scale bar is 100 μm.

An optical setup is prepared to investigate the characteristics of the LC q-Airy-plates. The setup is made up of a 632.8 nm He-Ne laser, a polarizer, a $\lambda/4$ plate, a sample stage, a spherical lens, and a CCD in sequence.[20] The incident light intensity and polarization state can be conveniently adjusted based on the combination of the polarizer and the $\lambda/4$ plate. The lens is set 125 mm (focal length) away from the sample to perform the Fourier transformation. After the q-Airy-plate samples are inserted in the optical path and work under proper applied voltage, the output VABs will be captured by the CCD. For simplicity, only the q(0.5)-Airy-plate is taken for further research.

When the incident light is left circularly polarized, a VAB with an orthogonal polarization, shown in Fig. 3(b), is observed at the propagation distance $D = 0$. This original observation point is defined as the focal plane of the lens. The experimentally measured intensity distribution is quite consistent with the simulation in Fig. 3(a), just like an Airy beam with a dark core inserted main lobe. The simulation is based on Eq. (3) under the half-wave condition. However, due to the residual phase of the LC sample,[30] the 0th order Gaussian beam over the main lobe, which corresponds to the first term in Eq. (3), cannot be totally suppressed. Nevertheless, the diffraction efficiency measured here has already reached at least 90%, which is significantly improved compared to existing techniques. It is interesting to note that the vortex part is not in a doughnut shape as the VABs appear in Refs. 16 and 19, in which the VABs are obtained through the combination of Airy beam generators and optical vortex generators, respectively. For the latter ones, as the generations of Airy beams or optical vortices are independent, the positions of the generators can be adjusted to ensure the doughnut-mode output. To verify the topological property of the vortex part in our work, astigmatic transformation[31] is employed and the converted pattern is shown in Fig. 3(c). The number and the tilting direction of the dark stripes between the transformed main lobes validate that the topological charge is +1. Moreover, dual orthogonally polarized VABs simultaneously appear under the linearly polarized illumination. The experimental result in Fig. 3(e) coincides well with the simulation in Fig. 3(d) except for the maximum of the light intensity, as the total energy of the former one is the same as that of single VAB in Fig. 3(b). A digital holographic imaging system[32] is applied to further test the phase singularities of the main lobes. As displayed in Fig. 3(f), spiral phases from 0 to 2π with opposite rotations are detected, denoting the +1 and −1 topological charges, respectively. This special phenomenon may add another degree of depth to the applications of VABs. Additionally, it is worth mentioning that, thanks to the electro-optical tunability of LCs,[24] the q-Airy-plates could work at the maximum wavelength of 2.0 μm (taking $\Delta n = 0.2$, $d = 5.0$ μm) via applying proper voltages, exhibiting good tolerance to the incident light wavelength.

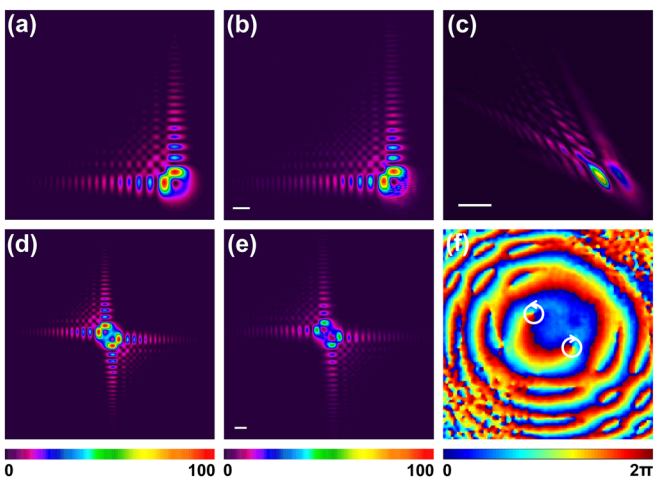

FIG. 3. (a) and (d) Simulated and (b) and (e) measured intensity distributions of single and dual VABs, respectively. (c) Astigmatic transformation pattern of (b). (f) Phase distribution of the central part of (e). The color bars for (a) to (e) indicate the relative optical intensity, and the color bar for (f) indicates the phase varying from 0 (blue) to 2π (red). The scale bar for all images is 300 μm.

Furthermore, the intensity distributions and transverse deflections of the single VAB at different distances are also measured to reveal the propagation dynamics. In Fig. 4, blue circles represent the experimental deflections of the center of mass, and the red line is the fitting curve showing a parabolic trajectory. Specifically, the inserted transverse profiles at corresponding distances vividly depict the dynamics along propagation. From the images, we can see that, despite the intensity distortion caused by the introduction of the optical vortex at the main lobe and surrounding positions, along with the propagation of VAB, the main lobe of the Airy beam is gradually reconstructed, indicating that the Airy beam still retains its self-healing property. Meanwhile, the optical vortex moves independently and will also reappear in the side lobe region. Besides, compared with the enlarged vortex beam, the lobes of the finite Airy beam are relatively diffraction-free. Therefore, the optical vortex and Airy beam propagate separately, keeping their intrinsic characteristics.

In conclusion, we propose and demonstrate LC q-Airy-plates via a SD1 and DMD based dynamic photo-patterning technique. The space-variant LC director distributions are integrations of corresponding q-plates and a PAM. In addition to a single VAB, dual VABs of orthogonal circular polarizations and opposite topological charges have also been generated with the polarization-controllable property. Topological charges of the optical vortices and transverse acceleration, self-healing, and nondiffraction of the Airy beam are

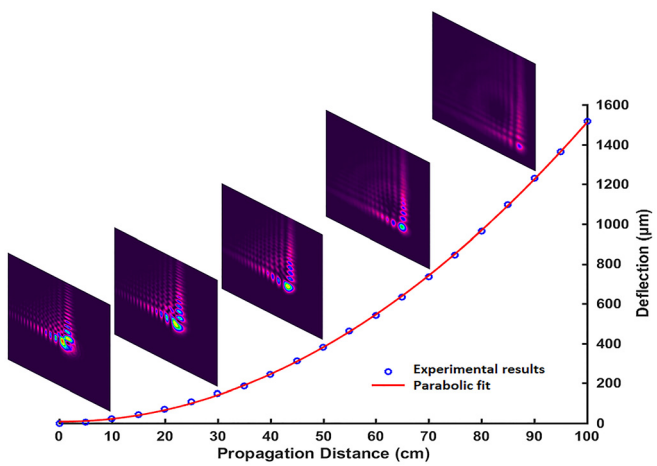

FIG. 4. Transverse acceleration of VAB as a function of propagation distance.

comprehensively investigated and verified. Moreover, the q-Airy-plates have advantages in a wide operating spectrum range, efficient modulation and low fabrication cost compared to previous approaches. This work supplies a compact configuration to generate high-quality and high-efficiency VABs and may pave the way for their potential applications in multidisciplinary fields.

This work was supported by the National Key R&D Program of China (2017YFA0303800), National Natural Science Foundation of China (NSFC) (11634010, 61377035, 61675168, and U1630125), and the Fundamental Research Funds for the Central Universities (3102017OQD103).

[1]A. M. Yao and M. J. Padgett, Adv. Opt. Photonics **3**, 161 (2011).
[2]L. Paterson, M. MacDonald, J. Arlt, W. Sibbett, P. Bryant, and K. Dholakia, Science **292**, 912 (2001).
[3]G. Molina-Terriza, J. P. Torres, and L. Torner, Nat. Phys. **3**, 305 (2007).
[4]L. Yan, P. Gregg, E. Karimi, A. Rubano, L. Marrucci, R. Boyd, and S. Ramachandran, Optica **2**, 900 (2015).
[5]J. Fischer and M. Wegener, Laser Photonics Rev. **7**, 22 (2013).
[6]J. H. Lee, G. Foo, E. G. Johnson, and G. A. Swartzlander, Jr., Phys. Rev. Lett. **97**, 053901 (2006).
[7]G. Siviloglou, J. Broky, A. Dogariu, and D. Christodoulides, Phys. Rev. Lett. **99**, 213901 (2007).
[8]J. Baumgartl, M. Mazilu, and K. Dholakia, Nat. Photonics **2**, 675 (2008).
[9]Y. Gu and G. Gbur, Opt. Lett. **35**, 3456 (2010).
[10]T. Vettenburg, H. I. Dalgarno, J. Nylk, C. Coll-Lladó, D. E. Ferrier, T. Čižmár, F. J. Gunn-Moore, and K. Dholakia, Nat. Methods **11**, 541 (2014).
[11]A. Chong, W. H. Renninger, D. N. Christodoulides, and F. W. Wise, Nat. Photonics **4**, 103 (2010).
[12]P. Polynkin, M. Kolesik, J. V. Moloney, G. A. Siviloglou, and D. N. Christodoulides, Science **324**, 229 (2009).
[13]S. W. Hell and J. Wichmann, Opt. Lett. **19**, 780 (1994); T. A. Klar and S. W. Hell, *ibid.* **24**, 954 (1999).
[14]J. Zhou, Y. Liu, Y. Ke, H. Luo, and S. Wen, Opt. Lett. **40**, 3193 (2015).
[15]M. Mazilu, J. Baumgartl, T. Cizmár, and K. Dholakia, Proc. SPIE **7430**, 74300C (2009).
[16]B. K. Singh, R. Remez, Y. Tsur, and A. Arie, Opt. Lett. **40**, 5411 (2015).
[17]H. Dai, Y. Liu, D. Luo, and X. Sun, Opt. Lett. **36**, 1617 (2011).
[18]R. Cao, Y. Yang, J. Wang, J. Bu, M. Wang, and X. C. Yuan, Appl. Phys. Lett. **99**, 261106 (2011).
[19]B. Y. Wei, P. Chen, S. J. Ge, W. Duan, W. Hu, and Y. Q. Lu, Appl. Phys. Lett. **109**, 121105 (2016).
[20]B. Y. Wei, P. Chen, W. Hu, W. Ji, L. Y. Zheng, S. J. Ge, Y. Ming, V. Chigrinov, and Y. Q. Lu, Sci. Rep. **5**, 17484 (2015).
[21]P. Chen, S. J. Ge, W. Duan, B. Y. Wei, G. X. Cui, W. Hu, and Y. Q. Lu, ACS Photonics **4**, 1333 (2017).
[22]J. Kim, *Liquid Crystal Geometric Phase Holograms for Efficient Beam Steering and Imaging Spectropolarimetry* (North Carolina State University, 2011).
[23]V. Chigrinov, S. Pikin, A. Verevochnikov, V. Kozenkov, M. Khazimullin, J. Ho, D. D. Huang, and H. S. Kwok, Phys. Rev. E **69**, 061713 (2004).
[24]B. Y. Wei, W. Hu, Y. Ming, F. Xu, S. Rubin, J. G. Wang, V. Chigrinov, and Y. Q. Lu, Adv. Mater. **26**, 1590 (2014).
[25]H. Wu, W. Hu, H. C. Hu, X. W. Lin, G. Zhu, J. W. Choi, V. Chigrinov, and Y. Q. Lu, Opt. Express **20**, 16684 (2012).
[26]P. Chen, B. Y. Wei, W. Ji, S. J. Ge, W. Hu, F. Xu, V. Chigrinov, and Y. Q. Lu, Photonics Res. **3**, 133 (2015).
[27]W. Ji, C. H. Lee, P. Chen, W. Hu, Y. Ming, L. Zhang, T. H. Lin, V. Chigrinov, and Y. Q. Lu, Sci. Rep. **6**, 25528 (2016).
[28]I. C. Khoo and S. T. Wu, *Optics and Nonlinear Optics of Liquid Crystals* (World Scientific, 1993).
[29]B. Y. Wei, P. Chen, S. J. Ge, L. C. Zhang, W. Hu, and Y. Q. Lu, Photonics Res. **4**, 70 (2016).
[30]X. W. Lin, W. Hu, X. K. Hu, X. Liang, Y. Chen, H. Q. Cui, G. Zhu, J. N. Li, V. Chigrinov, and Y. Q. Lu, Opt. Lett. **37**, 3627 (2012).
[31]V. Denisenko, V. Shvedov, A. S. Desyatnikov, D. N. Neshev, W. Krolikowski, A. Volyar, M. Soskin, and Y. S. Kivshar, Opt. Express **17**, 23374 (2009).
[32]S. Liu, L. Han, P. Li, Y. Zhang, H. Cheng, and J. Zhao, Appl. Phys. Lett. **110**, 171112 (2017).